1989

Order-disorder transition in capillary ripples

N. B. Tufillaro

R. Ramshankar

Jerry P. Gollub
Haverford College

Order-Disorder Transition in Capillary Ripples

N. B. Tufillaro,[a] R. Ramshankar, and J. P. Gollub
Department of Physics, Haverford College, Haverford, Pennsylvania 19041, and
Physics Department, University of Pennsylvania, Philadelphia, Pennsylvania 19104
(Received 3 October 1988)

A well-defined order-disorder transition occurs in the capillary waves on a fluid layer driven by vertical oscillation. The transition is characterized by a sharp decline in both the translational correlation length and the long-range orientational order of the pattern, and an onset in the characteristic frequency f^* of chaotic fluctuations varying approximately as $(A-A_d)^{1/2}$, for driving amplitudes above a threshold A_d. The transition is geometry dependent even when the container size is 50–100 times the wavelength.

PACS numbers: 47.20.Tg, 05.70.Fh, 47.35.+i

Instabilities in fluids often give rise to low-dimensional chaotic dynamics when the characteristic size λ of the typical spatial structure is comparable to the dimension L of the entire system. Examples of this phenomenon have been noted in studies of surface waves, Rayleigh-Benard convection, and other hydrodynamic systems.[1] The opposite case of chaotic dynamics in systems large compared to λ has more recently become the subject of intensive theoretical[2] and experimental[3] investigations. One current concept is that the dynamics of defects in otherwise regular patterns may be responsible for the development of complex dynamics.[4]

In this Letter, we report on a type of nonequilibrium order-disorder transition having some features of an equilibrium phase transition. The transition is observed in capillary ripples formed on a fluid surface subject to a vertical excitation. The excitation frequency is chosen so that the capillary wavelength λ is short compared to the system size. For rectangular geometries and driving amplitudes A somewhat above the onset of capillary waves, there exists a highly ordered and stable square-symmetric pattern [Fig. 1(a)]. At a well-defined second threshold A_d an order-disorder transition occurs that involves the formation of defects in the pattern, as has been noted qualitatively elsewhere.[5] A theoretical description in terms of amplitude equations has been proposed.[6]

Here we present quantitative measurements revealing the following features of the transition. Over a narrow interval in A, the correlation length ξ falls from a value comparable to the size of the system to a small value $\xi \leq \lambda$. The long-range orientational order in the pattern decreases substantially, and exhibits large fluctuations in the transition region. Finally, a characteristic frequency for the pattern fluctuation varies approximately as $(A-A_d)^{0.5}$. The phenomena depend on the geometrical symmetry of the container.

The experimental apparatus used to excite capillary ripples is similar to one described elsewhere.[7] An 8-cm square Plexiglass container of depth 2 cm is filled with *n*-butyl alcohol to a depth of 1 cm. The experiments are conducted at 30 °C. The cell is excited vertically with an electromagnetic shaker driven by a frequency synthesizer. Harmonics in the driving amplitude are negligible. The forcing frequency is 320 Hz and the dominant capillary wave frequency is the subharmonic[8,9] at 160 Hz. Similar phenomena to those described in this Letter are observed for excitation frequencies between 150 and 500 Hz.

The surface of the liquid is visualized by projection of a collimated white-light beam through the cell onto a diffusely scattering Mylar sheet fastened to the top cover of the cell. The patterns produced by refraction are then sampled locally by photodiodes, and globally with a video camera and digital imaging system (512×480 pixels). Images are typically taken from the central 20% of

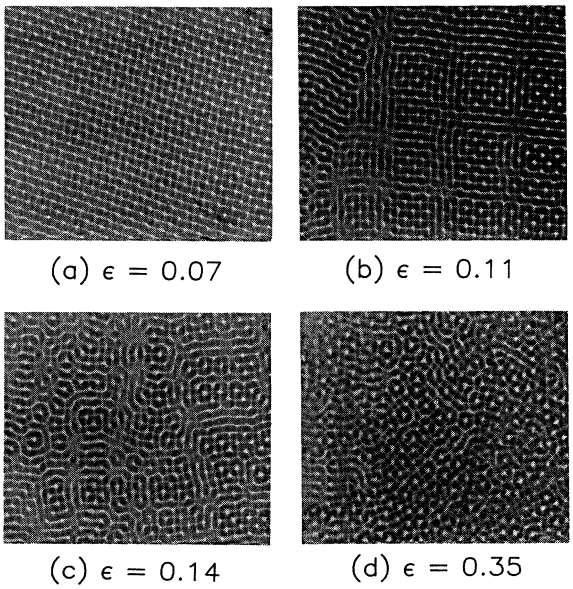

FIG. 1. Images of capillary wave patterns for four driving amplitudes $\epsilon=(A-A_c)/A_c$, where A_c is the threshold for waves. The region shown, about 20% of the cell, is 3.5×3.3 cm^2.

the cell area. The excitation amplitude, the primary control parameter, is measured in normalized units $\epsilon = (A - A_c)/A_c$, where A_c represents the onset amplitude for the waves.

Capillary ripple patterns for various excitation amplitudes are shown in Fig. 1. The ordered regime is illustrated in Fig. 1(a), for $\epsilon = 0.03$. The pattern of standing waves is generally not perfectly aligned with the system boundaries, which are outside the field of view in Fig. 1. Long-wavelength modulations are visible at a slightly higher amplitude as shown in Fig. 1(b) for $\epsilon = 0.11$. These modulations are believed to arise from a sideband instability.[6] Where they intersect, the wave amplitude can become small, thus providing a mechanism for defect formation. When sufficiently dense, the defects lead to destruction of the orientational order in the pattern [Fig. 1(c)]. At higher ϵ, the patterns are completely disordered.

To investigate this process quantitatively the two-dimensional discrete autocorrelation functions $C(x,y)$ of the images are computed.[10] Two examples corresponding to Figs. 1(a) and 1(c) are displayed in Fig. 2; the region shown corresponds to half the real space image. In the most ordered state, the envelope of $C(x,y)$ is almost independent of the radial displacement from the origin; the pattern shows long-range order. Just above the transition at A_d, on the other hand, the translational correlation length is comparable to λ.

In order to determine a correlation length ξ, we calculate the average absolute deviation from the mean of $C(m,n)$ (on a ring of radius r and thickness Δr), which we estimate by $\langle |\delta C| \rangle$. This function, which is a measure of the contrast or envelope of $C(x,y)$, may be satisfactorily fitted by an exponential function of r over the relevant range of excitation amplitudes. Examples of these fits for various excitation amplitudes are presented in Fig. 3(a). The resulting correlation length $\xi(\epsilon)$ is shown in Fig. 3(b). The dramatic decline near $\epsilon = 0.10$ is clearly evident.

Following the method used by Occelli, Guzzelli, and Pantaloni[11] on a different system, we also measure the degree of orientational order in the patterns by calculating the fourfold orientational correlation function of the kind first considered in the theory of two-dimensional melting.[12] It is computed by first locating all of the local maxima of the image intensity (these are the wave antinodes) and then connecting each point with its four nearest neighbors. The resulting network of line segments (with gaps at the locations of defects) is taken to represent the orientational relationships in the wave pattern. (Alternatively, the network could be created by Deluancey triangulation.[13]) We then define $\theta(\mathbf{r}')$ to be the orientation angle in the plane (relative to the x axis) of a line segment centered at $\mathbf{r}'$, and compute

$$G_4(r) = \langle \cos 4\{\theta(\mathbf{r}') - \theta(\mathbf{r}_0)\} \rangle ,$$

where the average is taken over all reference points $\mathbf{r}_0$ and points $\mathbf{r}'$ such that $|\mathbf{r}' - \mathbf{r}_0| = r$ (to within one pixel). This function measures the extent to which fourfold orientational order persists for separations comparable to r.

The resulting orientational correlation functions are presented in Fig. 4(a). After an initial falloff, $G_4(r)$ reaches a plateau that is approximately independent of r. This indicates the presence of long-range orientational order on a scale comparable to L. The height $\langle G_4 \rangle$ of the plateau (also averaged over time) declines sharply near $\epsilon = 0.10$, as shown in Fig. 4(b). The location of the order-disorder transition as manifested in $\langle G_4 \rangle$ is the same as that for ξ, as may be seen by the comparison of Fig. 4(b) with Fig. 3(b). (This behavior is in contrast to that found for two-dimensional melting.) During the transition, the density of defects also undergoes a rapid

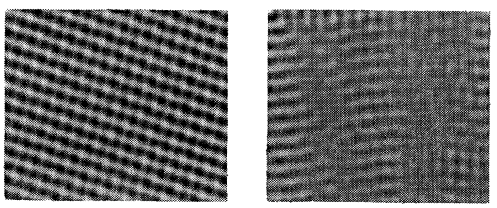

FIG. 2. Two-dimensional autocorrelation functions $C(x,y)$ for the patterns in Figs. 1(a) and 1(c). The origin is at the upper left.

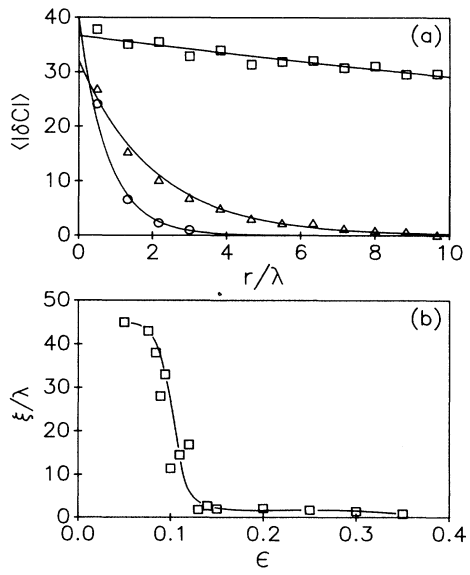

FIG. 3. (a) Average absolute deviation (qualitatively, the envelope or contrast) of the autocorrelation functions for three values of ϵ as a function of r/λ ($\epsilon = 0.07$, squares; $\epsilon = 0.15$, triangles; $\epsilon = 0.35$, circles). (b) Correlation length ξ as a function of ϵ.

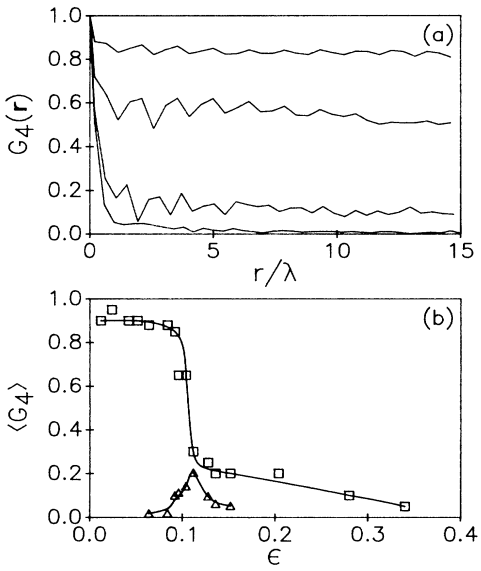

FIG. 4. (a) Orientational correlation functions $G_4(r)$ for the patterns shown in Fig. 1, as a function of r/λ. (b) Average height of the plateau in $G_4(r)$ as a function of ϵ (squares). The triangles show the rms fluctuation in the plateau height as a function of ϵ. The transition occurs near $\epsilon=0.010$ as in Fig. 3(b).

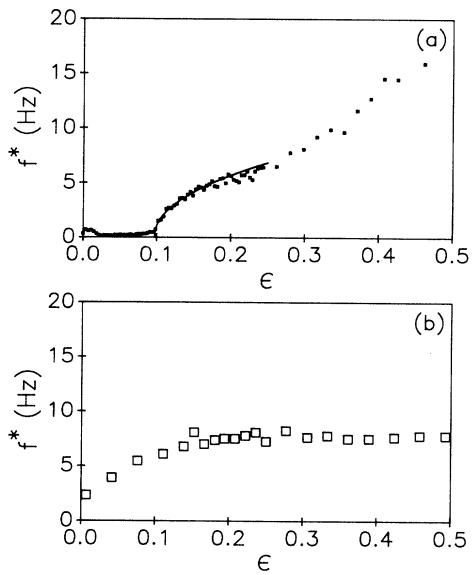

FIG. 5. (a) Inverse f^* of the autocorrelation time, as a function of ϵ, for the large square cell. The characteristic fluctuation frequency increases sharply at the threshold ϵ_d of the spatial order-disorder transition. (b) Same for a circular cell of identical area. The square pattern is intermittent, and there is no sharp transition.

increase, but quantitative measurements of the defect density are difficult to make.

In the region of the transition $\langle G_4 \rangle$ fluctuates substantially in time because of the large size of the correlation length, whereas farther above the transition the fluctuations become small. These fluctuations arise from the large size of the correlation length in the transition region. We have measured the fluctuations by computing the root mean square deviation of the plateau height $\langle G_4 \rangle$ over approximately sixteen patterns at each value of ϵ. The result is also displayed in Fig. 4(b).

Finally, it is interesting and important to compare the spatial measurements to the time evolution of the pattern as determined by a local probe in the optical image. The time series has a broad spectrum and is chaotic but does not have a small attractor dimension. We compute the temporal autocorrelation function, and use the time to the first half-maximum as a measure of the characteristic time of the pattern fluctuations. The inverse f^* of this time is plotted as a function of ϵ in Fig. 5(a). In the ordered region, the only time dependence is due to a slow drift in the overall pattern at the rate of about 0.3 mm/s. This gives a finite but small value of f^* below the transition. As ϵ is increased beyond $\epsilon_d=0.097\pm0.004$, f^* increases sharply, and is well approximated up to $\epsilon=0.25$ by the function $f^*=B(\epsilon-\epsilon_d)^\gamma$, where $\gamma=0.47\pm0.07$. For larger ϵ, f^* increases more rapidly and the pattern is completely disordered.

These phenomena are significantly dependent on the geometry of the container, even though $L\gg\lambda$. In both circular and triangular cells the square pattern still predominates, but is intermittent as a result of defects originating *from the wall*. (In the rectangular geometry *internally generated* defects destabilize the pattern, but only for $\epsilon>0.1$.) Furthermore, there is no sharp transition in these other geometries, as shown in Fig. 5(b). The destabilization associated with the circular geometry may be similar to that found in thermal convection.[14]

It is noteworthy that the transition in the characteristic frequency of chaotic fluctuations [Fig. 5(a)] coincides with the onset of spatial disorder (Figs. 3 and 4). These chaotic fluctuations result from a different mechanism than that seen in simple dynamical systems or small aspect ratio fluid systems, i.e., the lack of correlation between many discrete regions which are not separately chaotic. This behavior is possibly an example of "defect mediated turbulence."[4] The observation of a well-defined order-disorder transition in this system is unexplained at the present time. However, a sharp transition to chaos has recently been noted in the mean-field theory of a continuous-time dynamic network model in the infinite-size limit.[15]

Spatial and temporal correlation techniques seem to be appropriate methods for characterizing large aspect ratio chaotic systems statistically, just as they are for equilibrium condensed-matter physics and for conventional turbulence. It will be necessary to study larger systems to understand clearly what features are retained as the ratio L/λ becomes very large. For example, though the translational correlation functions are satis-

factorily described by exponentials, the present measurements cannot positively exclude algebraic decay at large distances in the ordered regime.

This work was supported by the University Research Initiative program under Contract No. DARPA/ONR N00014-85-K-0759 to Princeton University. N.B.T. was supported by the National Science Foundation under Grant No. MSM-8310933 to Haverford College. The importance of measuring the correlation length was pointed out to us by P. Hohenberg. We also appreciate helpful discussions with and assistance from T. Solomon and A. Dougherty.

---

[a]Currently at Physics Department, University of Otago, Dunedin, New Zealand; also affiliated with Bryn Mawr College, Bryn Mawr, PA 19010.

[1]For references, see H. L. Swinney, Physica (Amsterdam) **7D**, 3 (1983). Chaos in surface waves has been documented experimentally by S. Ciliberto and J. P. Gollub, J. Fluid Mech. **158**, 381 (1985) and theoretically by E. Meron and I. Procaccia, Phys. Rev. A **56**, 1323 (1986).

[2]See, for example, P. Coullet, C. Elphick, and D. Repaux, Phys. Rev. Lett. **58**, 431 (1987); T. Bohr, G. Grinstein, Y. He, and C. Jayaprakash, Phys. Rev. Lett. **58**, 2155 (1987); H. Chate and P. Manneville, Phys. Rev. Lett. **58**, 112 (1987); A. C. Newell in *Propagation in Nonequilibrium Systems,* edited by E. Wesfried and H. Brandt (Springer-Verlag, Berlin, 1988).

[3]See, for example, S. Douady and S. Fauve, Europhys. Lett. **6**, 221 (1988); S. Ciliberto and P. Bigazzi, Phys. Rev. Lett. **60**, 286 (1988); C. W. Meyer, G. Ahlers, and D. S. Cannell, Phys. Rev. Lett. **59**, 1577 (1987); I. Rehberg and V. Steinberg, to be published.

[4]P. Coullet, L. Gil, and J. Lega, to be published; L. Gil, J. Lega, and J. L. Meunier, to be published.

[5]A. B. Ezerskii, P. I. Korotin, and M. I. Rabinovich, Pis'ma Zh. Eksp. Teor. Fiz. **41**, 129 (1985) [JETP Lett. **41**, 157 (1985)].

[6]A. B. Ezerskii, M. I. Rabinovich, V. P. Reutov, and I. M. Starobinets, Zh. Eksp. Teor. Fiz. **91**, 2070 (1986) [Sov. Phys. JETP **64**, 1228 (1986)].

[7]F. Simonelli and J. P. Gollub, J. Fluid Mech. (to be published).

[8]Lord Rayleigh, Philos. Mag. **5**, 50 (1883).

[9]For a review of parametrically excited surface waves, see V. G. Nevolin, J. Eng. Phys. (USSR) **47**, 1028 (1984).

[10]X. Gonzalez and Z. Wintz, *Digital Image Processing* (Addison-Wesley, Reading, MA, 1977).

[11]R. Occelli, E. Guzzelli, and J. Pantaloni, J. Phys. (Paris) Lett. **44**, L567 (1983).

[12]D. R. Nelson, in *Phase Transitions and Critical Phenomena,* edited by C. Domb and M. S. Green (Academic, London, 1983), Vol. 7.

[13]D. T. Lee and B. J. Schacter, Int. J. Comput. Inform. Sci. **9**, 219 (1980); P. J. Green and R. Sibson, Comput. J. **21**, 168 (1978).

[14]V. Croquete, "Convective Pattern Dynamics at Low Prandtl Number" (to be published).

[15]H. Sompolinsky, A. Crisanti, and H. J. Sommers, Phys. Rev. Lett. **61**, 259 (1988).

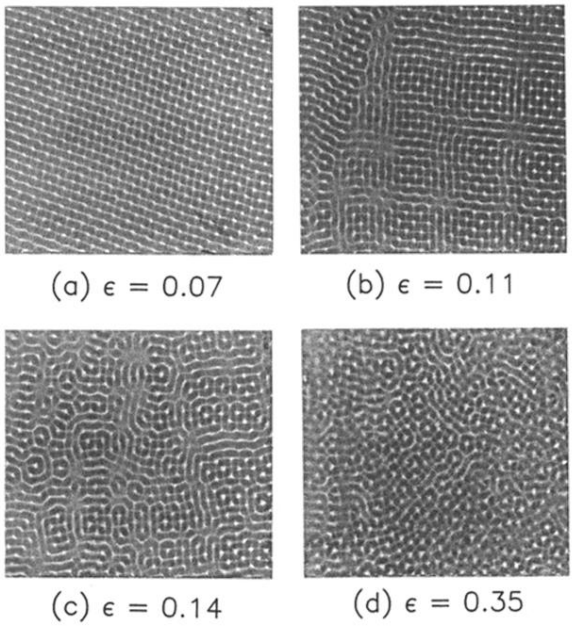

FIG. 1. Images of capillary wave patterns for four driving amplitudes $\epsilon=(A-A_c)/A_c$, where A_c is the threshold for waves. The region shown, about 20% of the cell, is 3.5×3.3 cm^2.

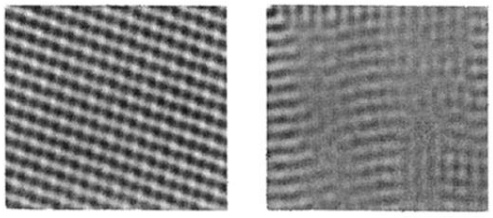

$\epsilon = 0.07$ $\epsilon = 0.14$

FIG. 2. Two-dimensional autocorrelation functions $C(x,y)$ for the patterns in Figs. 1(a) and 1(c). The origin is at the upper left.